Theory of the skyrmion, meron, antiskyrmion, and antimeron in chiral magnets

Sandip Bera[1] and Sudhansu S. Mandal[1,2]

[1]*Department of Physics, Indian Institute of Technology, Kharagpur 721302, India*
[2]*Centre for Theoretical Studies, Indian Institute of Technology, Kharagpur 721302, India*

We find closed-form solution of the Euler equation for a chiral magnet in terms of a skyrmion or a meron depending on the relative strengths of magnetic anisotropy and magnetic field. We show that the relevant length scales for these solutions primarily depend on the strengths of Dzyaloshinskii-Moriya interaction through its ratios, respectively, with magnetic field and magnetic anisotropy. We thus unambiguously determine the parameter dependencies on the radius of the topological structures particularly of the skyrmions, showing an excellent agreement with experiments and first-principles studies. An anisotropic Dzyaloshinskii-Moriya interaction suitable for thin films made with C_{nv} symmetric materials is found to stabilize antiskyrmion and antimeron, which are prototypical for D_{2d} symmetric systems, depending on the degree of anisotropy. Based on these solutions, we obtain a phase diagram by comparing the energies of various collinear and noncollinear competing phases.

I. INTRODUCTION

The chiral Dzyaloshinskii-Moriya interaction (DMI) [1,2] for broken inversion symmetric systems is one of the most important mechanisms including frustrated exchange interactions and long-ranged dipolar interaction for producing one-dimensional modulation in magnetization known as spin spiral [3–9] in ferromagnetic systems. An application of magnetic field in such a system stabilizes [7,10] skyrmions (Sks) having topologically protected quasiparticlelike spin structure [11–16] in a ferromagnetic background. Néel- and Bloch-type Sks are generally realized, respectively, in C_{nv} and D_n symmetric [3,10] bulk and thin-film materials for wide range of magnetic fields and temperatures [11–21].

Recent observations [22,23] of antiskyrmions (ASks) in Heusler alloys with D_{2d} crystal symmetry have raised an issue about the microscopic environment, which will stabilize a Sk or an ASk. While a Sk has either Néel or Bloch type of orientation of magnetization vector governed by the respective transverse and longitudinal DMI, an ASk displays a combination of both. It is thus tempting to think that an antiskyrmion may be produced in a crystal whose symmetry gives rise to both types of DMI. Numerical simulations, on the contrary [24–26], indicate that the ASks do stabilize only in the presence of dipolar interaction. A micromagnetic study [27] suggests that Sks and ASks can, however, coexist and this coexistence is predicted by electronic structure calculation at interfaces due to anisotropic DMI. These ASks even take part in current-induced motion [28].

Hoffmann *et al.* [27] have recently observed ASks in C_{2v} symmetric systems grown on semiconductor or heavy-metal substrates, while C_{nv} symmetric systems are known to stabilize Sks only [3,7]. This motivates us to study a system of thin-film chiral magnet that may be fabricated with C_{nv} symmetric crystals with an anisotropic DMI in a continuum model in search of ASk solution. Camosi *et al.* [29] have recently reported that the epitaxially grown thin Co films on W(110) brings anisotropy in DMI along two orthogonal growth directions of a C_{2v} symmetric bulk system. Although this reported anisotropy does not correspond to two opposite signs along two orthogonal directions, a micromagnetic simulation seems to suggest anisotropy in thin films not only in magnitude but also in sign [28]. We introduce a model DMI with such an anisotropy.

Moreover, recent observation of another topological spin structure, viz, meron [30,31] have further raised the theoretical issue on the parameter regimes on which all these different kinds of topological structures emerge. Further, definite parameter dependencies on the radius [32–35] and appropriate length scale [7] of a Sk are not yet settled. Our focus is thus solving basic Euler equation for angular variables representing magnetization with isotropic DMI for Sks and merons and then study the consequences of its anisotropy followed by the determination of phase diagram by comparing energies of different possible solutions for thermodynamically stable magnetic structures.

In this paper, we solve the Euler equation in a continuum model [3,7] with ferromagnetic exchange coupling, J, DMI strength, D, strength of magnetic anisotropy, A, and net Zeeman energy due to magnetic field, H. For moderate to high HJ/D^2 and $\gamma = 2A/H < 1$, we find that the relevant length scale of the corresponding skyrmion solution is $r_s = D/H$, contrasting the belief [36] of the relevant length scale $r_d = J/D$. This enables us to determine the magnetic field and anisotropy dependencies of the radius of a skyrmion and

find that it is in excellent agreement with experiments [32,37] and first-principles studies [33]. The meron solution at zero magnetic field is obtained for $A > 0$ (easy-plane anisotropy) by minimizing energy and the relevant length scale is found to be D/A. We show the formation of meron lattice and argue how a symmetric Sk is evolved from a meron via an asymmetric skyrmion, explaining a recent experiment as well as simulation results [31]. Further, our model with an anisotropic DMI is shown to stabilize ASks and antimerons in C_{nv} symmetric systems, as evident in recent realization [27] of ASks in C_{2v} symmetric systems. We finally determine phase diagram for $\gamma < 1$ by comparing energies of the skyrmion solution with other collinear and noncollinear competing phases.

II. GENERAL DESCRIPTION OF SKYRMION AND ANTISKYRMION

We begin with considering a two-dimensional chiral magnet having energy $E = \int d^2r (\mathcal{E}_{EX} + \mathcal{E}_{DM}^{\pm} + \mathcal{E}_{AH})$ with respect to an overall ferromagnet orienting along perpendicular to the plane of the system, described by exchange energy density $\mathcal{E}_{EX} = \frac{J}{2}(\nabla \hat{m})^2$, DMI energy density $\mathcal{E}_{DM}^{\pm} = -D(L_{xz}^{(x)} \pm L_{yz}^{(y)})$. Here $L_{ij}^{(k)} = \hat{m}_i \partial_{x_k} \hat{m}_j - \hat{m}_j \partial_{x_k} \hat{m}_i$, $\hat{m}$ is unit magnetization vector, $\pm$ signs, respectively, refer to the systems with C_{nv} and D_{2d} symmetries when the Dzyaloshinskii-Moriya vector is transverse [38] to the lattice bond. (While the former supports Sks the later is suitable for stabilizing ASks.) The energy density for magnetic anisotropy and applied magnetic field along $\hat{z}$ direction given by $\mathcal{E}_{AH} = -A(1 - \hat{m}_z^2) + H(1 - \hat{m}_z)$, where $A > 0 (< 0)$ refers to easy-plane (easy-axis) anisotropy. In spherical polar representation,

$$\hat{m}(\boldsymbol{r}) = [\cos \Phi(\boldsymbol{r}) \sin \Theta(\boldsymbol{r}), \ \sin \Phi(\boldsymbol{r}) \sin \Theta(\boldsymbol{r}), \ \cos \Theta(\boldsymbol{r})]$$

with $\boldsymbol{r} = (r \cos \phi, r \sin \phi)$ in polar coordinate system.

A topological structure defined by its topological quantum number $N_{sk} = \frac{1}{4\pi} \int d^2r \, \hat{m} \cdot (\partial_x \hat{m} \times \partial_y \hat{m}) \equiv \pm N_0$, where positive sign refers to a Sk or meron and negative sign refers to an ASk or antimeron. The solutions [7] of a Sk/meron and an ASk/antimeron correspond to $\Theta(\boldsymbol{r}) = \Theta(r)$ and, respectively, $\Phi(\boldsymbol{r}) = \pm \phi + \eta$. Here η determines a constant extra planar rotation of magnetic moment at all points; $\eta = 0 (\pi/2)$ for Néel- (Bloch)-type topological structures. Here N_0 represents the winding number [36]: its positive (negative) sign determines inward (outward) spin orientation with respect the origin, corresponding to negative (positive) sign of D, and its magnitude is 1 for Sks and ASks, and $1/2$ for merons and antimerons. The boundary condition, $\hat{m} = (0, 0, +1)$ for $r \to \infty$, i.e., $\Theta(r \to \infty) = 0$ and $\hat{m} = (0, 0, -1)$ at $r = 0$, i.e., $\Theta(r = 0) = \pi$ is for both Sk and ASk. Meron and antimeron correspond to the boundary condition $\Theta(r = \infty) = \pi/2$ and $\Theta(r = 0) = \pi (0)$ for inward (outward) helicity.

No matter, be it C_{nv}, D_{2d}, or D_n systems, the Euler equation for $\Theta(r)$ is identical (see Appendix A). By introducing a length scale $r_s = D/H$ and rescaling $r \to r_s \rho$, we obtain (see Appendix A) the Euler equation

$$\frac{d^2\Theta}{d\rho^2} + \frac{1}{\rho}\frac{d\Theta}{d\rho} - \frac{\sin\Theta\cos\Theta}{\rho^2}$$
$$= \frac{H_0}{H}\left(-\frac{2}{\rho}\sin^2\Theta + \sin\Theta - \gamma\sin\Theta\cos\Theta\right), \quad (1)$$
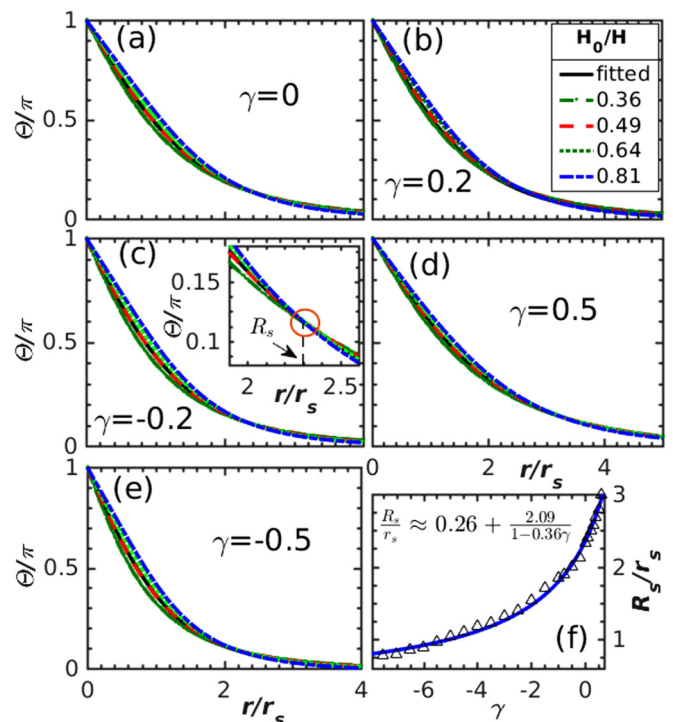

FIG. 1. Skyrmion or antiskyrmion solution: Numerical solution of the Euler equation (1), i.e., $\Theta(r)$ vs. r/r_s for different values of γ in (a)–(e) for same set of H_0/H, viz, 0.36, 0.49, 0.64. and 0.81. Solid lines represent the best fit solution with the form given by Eq. (2). Inset in (c) is a representative of (a)–(e) for showing the crossing of the curves for different values of H_0/H. Also see Appendix A for wider range of parameters. The differences in profiles of Θ for different H/H_0 are minimal beyond this interception point, which is identified as the radius, R_s, of a skyrmion. The dependence of R_s on γ along with its approximate fitted form is shown in (f).

where $H_0 = D^2/J$ and $\gamma = 2A/H$. The numerical solutions of the Eq. (1) with the boundary conditions $\Theta(0) = \pi$ and $\Theta(\infty) = 0$ for different values of H_0/H and γ are shown in Fig. 1. The length scale r_s, which is independent of exchange energy J defines the relevant length scale as for a fixed value of γ, the deviation of the curves of $\Theta(r)$ for different values of H_0/H are almost negligible; the complete solution of Eq. (1) is thus best approximated by

$$\Theta(r) = 4\arctan[\exp(-\beta(\gamma)r/r_s)] \quad (2)$$

with $\beta(\gamma) \approx 0.91 - 0.55\gamma$.

We note that all the curves for a fixed γ cross [see inset of Fig. 1(c)] at a particular r and we identify that to be the radius, R_s, of a Sk. We find its dependency on γ as $R_s = r_s w(\gamma)$ with $w(\gamma) \approx 0.26 + \frac{2.09}{1-0.36\gamma}$. Therefore, the magnetic field dependence of the radius of a Sk may be parametrized as

$$R_s = \frac{C_1}{H} + \frac{C_2}{H - C_3}, \quad (3)$$

where the coefficients C_1 and C_2 are proportional to $|D|$ and C_3 is proportional to A. We note that for a fixed H, radius of a Sk increases with positive A, in agreement with an experiment [37]. However, an increase of easy-axis anisotropy will reduce the size of an Sk. Figure 2 shows that the skyrmion radius
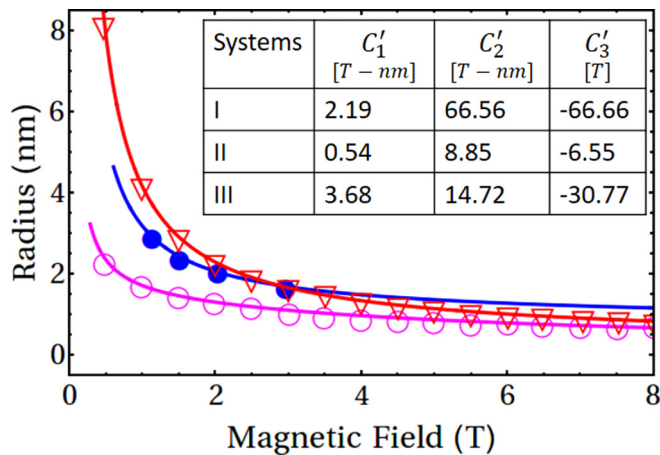
FIG. 2. Variation of radius of a Sk with applied magnetic field: Experimental data (solid circles) from Ref. [32], first-principles calculations from Ref. [33] for hcp lattice (open circle) and fcc lattice (open inverted triangles), denoted, respectively, as I, II, and III. Solid lines are the fitted curves of these data with the functional form in Eq. (3). Inset: Coefficients obtained by fitting are tabulated where we have put primes to distinguish from nonprimes in Eq. (3) in view of dimensions.

obtained in an experiment [32] and first-principles studies [33] obey the relation (3) very well and the sign of the corresponding fitted C_3 are consistent with the sign of the reported A. For the systems with positive A, lower bound of the magnetic field needed for producing a Sk is $H_{lb} = 2A$ and thereafter the radius monotonically decreases with increasing H.

III. PHASE DIAGRAM

Figure 3(a) shows phase diagram in A–H space with $\gamma < 1$. The phase boundary between skyrmion and the polarized ferromagnet is determined by comparing energy of a Sk,

$$E_{sk} = 2\pi \int_0^\infty dr\, r \left[\frac{J}{2} \left(\left(\frac{d\Theta}{dr} \right)^2 + \frac{\sin^2 \Theta}{r^2} \right) - A \sin^2 \Theta \right.$$
$$\left. + D \left(\frac{d\Theta}{dr} + \frac{\sin \Theta \cos \Theta}{r} \right) + H(1 - \cos \Theta) \right] \quad (4)$$

with the energy of the ferromagnet. Similarly by determining energy of a spin-spiral following Ref. [3] in comparison to the ferromagnet, we obtain the phase boundary between the spin spiral and ferromagnet. We draw phase boundary between spin-spiral and skyrmion phases by considering maximum possible phase space for spin-spiral structure. The phase diagram for $\gamma < 1$ here is consistent with previously reported phase diagrams obtained by variational and other simulations [39,40]. In agreement with an experiment [41], both spin spiral and skyrmions are accessible at zero anisotropy.

IV. MERON SOLUTION

For a sufficiently high easy-plane anisotropy ($A > 0$) and $H = 0$, all the spins will align in the plane (planar ferromagnet). This indicates a boundary condition $\Theta(\infty) = \pi/2$, which together with another boundary condition $\Theta(0) = 0$
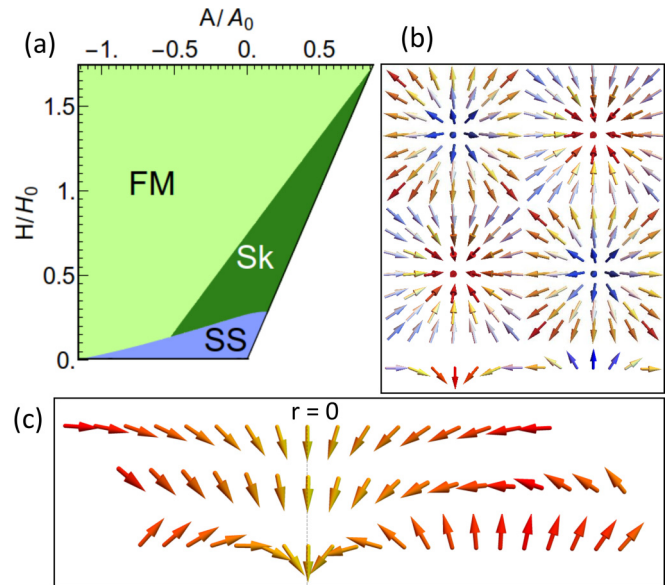

FIG. 3. (a) Phase diagram in A/A_0–H/H_0 space, where $A_0 = H_0 = D^2/J$. Three distinct phases: spin-spiral (SS), isolated skyrmion (Sk), and polarized ferromagnet (FM) whose magnetization direction is along the applied H. The right boundary corresponds to $\gamma = 1$. (b) Two possible degenerate structures of merons (up or down spin at the center) for $H = 0$. From top, two- and one-dimensional spin-structures of merons. Any finite H stabilizes meron with down-spin at the center only. (c) From top, depiction of a symmetric meron ($H = 0$), an asymmetric meron ($H > 0$, $\gamma > 1$), and an asymmetric skyrmion. Spin-down at $r = 0$ for all these structures. Here the schematics (b), (c) of merons and skyrmion are considered for $D < 0$.

or π will provide a solution of meron when A is moderate. Taking cue of the skyrmion solution, we assume the solutions of meron (see Appendix B) to be

$$\Theta(r) = \pm \frac{\pi}{2} + 2 \arctan[\exp(-\zeta r/r_a)], \quad (5)$$

where $r_a = D/A$ is the characteristic length scale, positive (negative) sign corresponds to spin down (up) at the center of the meron, and the parameter ζ to be determined by minimizing its energy

$$E_{meron} = 2\pi \int_0^\infty r\, dr \left[\frac{J}{2} \left(\left(\frac{d\Theta}{dr} \right)^2 + \frac{\sin^2 \Theta}{r^2} \right) \right.$$
$$\left. + A \cos^2 \Theta + D \left(\frac{d\Theta}{dr} + \frac{\sin \Theta \cos \Theta}{r} \right) \right]. \quad (6)$$

We find (see Appendix B) $\zeta = 2 \ln(2)/(1 + 2G) \approx 0.49$, where G is Catalan's constant. These solutions of $\Theta(r)$ are degenerate and hence they occur simultaneously and appear as neighbors to match the background of planar ferromagnet and form a meron lattice, as shown in Fig. 3(b). However, with the increase of H, only one kind of meron (spin down at its core) survives as the other will have higher energy, because the background of spin alignment will have nonzero out of plane (up) component. For further increase of H, this meron gradually converts into a skyrmion as it helps to orient

more spin with finite up component. This is reminiscent of the recently observed merons by Yu *et al.* [31]. We estimate the upper bound of A for forming a meron as $A_{ub} \approx 2.3A_0$ by comparing the energy of a meron and the planar ferromagnet.

In the presence of H with $A \gg 0$ such that $\gamma > 1$, a tilted ferromagnet will be formed with finite amount of spin projection along the direction of H making a tilting angle $\arccos(1/\gamma)$ with the plane. With such a tilted ferromagnet in the background, locally formed merons with down spin at its core will be asymmetric as shown schematically in Fig. 3(c) when $A < A_{ub}$. If we look along a particular direction, a meron's spin alignment at one boundary will be along the tilting angle $\arccos(1/\gamma)$ and at the other boundary it will differ by an angle π. This makes the meron asymmetric. We note that actual A_{ub} may be lower than estimated here because of the predicted possibility of forming cone-like structure in the intermediate regime. The cone structure [39,40] and the tilted ferromagnet are indistinguishable in our analysis because both these structures correspond to same Θ. With further increase of H, some more spins will tend to align more than $\arccos(1/\gamma)$ forming an asymmetric skyrmion [Fig. 3(c)], corroborated with the recent numerical simulation result [42]. Upon further increase of H, right (left) side of the Sk becomes shorter (longer) and evolve into a symmetric Sk at $\gamma = 1$ as we enter into the Sk phase of the phase diagram [Fig. 3(a)].

V. ANTISKYRMION AND ANTIMERON

In search of ASk and antimeron in thin films made of C_{nv} symmetric systems [43], we introduce an anisotropic DMI given by

$$\mathcal{E}_{DM}^+ = -D(1 + \lambda \cos 2\phi)\left(L_{xz}^{(x)} + L_{yz}^{(y)}\right). \quad (7)$$

Here λ denotes the degree of anisotropy with $\lambda = 0$ representing the symmetric DMI present in the bulk C_{nv} symmetric crystals. The energy of an ASk is then found to be

$$E_{ask} = 2\pi \int_0^\infty dr\, r \left[\frac{J}{2}\left(\left(\frac{d\Theta}{dr}\right)^2 + \frac{\sin^2\Theta}{r^2}\right) - A\sin^2\Theta \right.$$
$$\left. + \frac{\lambda}{2}D\left(\frac{d\Theta}{dr} - \frac{\sin\Theta\cos\Theta}{r}\right) + H(1 - \cos\Theta) \right] \quad (8)$$

with $\Theta(r)$ given in Eq. (2). Inset of Fig. 4(a) shows the variation of E_{ask} with λ for $A = 0$ and we find that $E_{ask} < E_{sk}$ above a critical value $\lambda_c \approx 1.4$ and hence the anisotropy in DMI stabilizes an ASk. A phase diagram has been presented in Fig. 4(a). Ferromagnet to ASk transition is also possible for $\lambda > \lambda_c$, and the corresponding critical value increases with H. However, ASks are not possible for lower H/H_0 where spin-spiral phase remains unaltered for any λ. Figure 4(b) shows minimum values of λ above which the full phase space of Sks and partial phase of ferromagnets shown in Fig. 3(a) can stabilize ASks. The outer boundary in the ferromagnetic region is obtained with the criterion that the ratio of the diameter of an ASk and the spin-spiral wavelength is not less than 0.4.
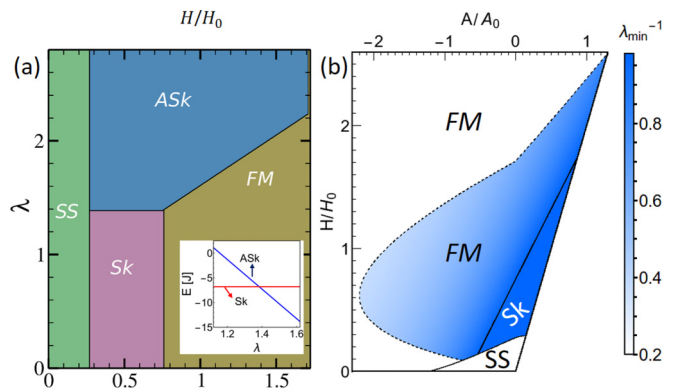

FIG. 4. (a) Phase diagram in H/H_0–λ plane when $A = 0$. Four distinct phases are obtained by comparing their energies. While the energies of a skyrmion and an antiskyrmion have been calculated using the expressions (4) and (8), respectively, the energy of the spin-spiral phase has been obtained following the procedure reported in Ref. [3]. The inset shows comparison of the energies of a Sk and an ASk with respect to the energy of the ferromagnetic ground state in the background as a function of anisotropy parameter λ of DMI. The crossing point of two lines determines the boundary between skyrmionic and antiskyrmionic phases. (b) The color map indicates minimum value of λ above which an ASk is stabilized over a Sk or a ferromagnet in the parameter space shown in Fig. 3(a).

The energy of an antimeron in presence of anisotropic DMI,

$$E_{anti-meron} = 2\pi \int_0^\infty r\,dr \left[\frac{J}{2}\left(\left(\frac{d\Theta}{dr}\right)^2 + \frac{\sin^2\Theta}{r^2}\right) \right.$$
$$\left. + A\cos^2\Theta + \frac{\lambda}{2}D\left(\frac{d\Theta}{dr} - \frac{\sin\Theta\cos\Theta}{r}\right) \right] \quad (9)$$

becomes less than E_{meron} for $6.8 \lesssim \lambda$. Producing antimerons by anisotropic DMI is less probable than producing ASk because the former requires much higher degree of anisotropy, which is almost in the verge of the limit of a D_{2d} system.

VI. CONCLUSION

We here have shown that the anisotropic DMI in thin films with C_{nv} symmetric materials can host antiskyrmions for wide range of phase space of A and H, in comparison to hosting skyrmions. However, we do not find any regime of the coexistence of Sks and ASks, in contrast to the numerical simulation [27]. Although dipolar interaction is also a suitable mechanism [24–26] for stabilizing ASks, the anisotropic DMI is solely responsible, to the best of our knowledge, for small-size ASks in C_{nv} symmetric systems. The dipolar interaction here may play a role in reducing [44] the effect of magnetic anisotropy. The physics of Sk/ASk and meron/antimeron discussed here will reverse for systems with D_{2d} symmetries. Although the structure of an antiskyrmion is a combination of the structures of Néel- and Bloch-type Sks, which are prototypical, respectively, of DMI with Dzyaloshinskii-Moriya vector orthogonal to the neighboring bond and along the bond, their combinations do not produce ASks. However, a pure D_n symmetric system will stabilize Bloch-type merons and

Sks, and the corresponding antimerons and ASks may also be produced through anisotropic DMI.

APPENDIX A: EULER EQUATION AND ITS SKYRMION SOLUTION

Energy for a two-dimensional chiral magnet is given by

$$E = \int d^2r \left[\frac{J}{2}(\nabla\hat{m})^2 + \mathcal{E}_{DM} + H(1 - \hat{m}_z) - A(1 - \hat{m}_z^2) \right],$$
(A1)

where energy density for DMI, $\mathcal{E}_{DM} = -D(L_{xz}^{(x)} + L_{yz}^{(y)})$ for C_{nv} symmetric, $-D(L_{yz}^{(x)} + L_{zx}^{(y)})$ for D_n symmetric and $-D(L_{xz}^{(x)} - L_{yz}^{(y)})$ for D_{2d} symmetric systems and we distinguish them by introducing a parameter α with respective values 1, 2, and -3. Unit magnetization can be parametrized through spherical variables (Θ, Φ) as

$$\hat{m}(\mathbf{r}) = [\cos\Phi(\mathbf{r})\sin\Theta(\mathbf{r}), \sin\Phi(\mathbf{r})\sin\Theta(\mathbf{r}), \cos\Theta(\mathbf{r})]$$

with $\mathbf{r} = (r\cos\phi, r\sin\phi)$ in polar coordinate. Therefore, the expression of energy reduces to

$$E = \int_0^\infty r\,dr \int_0^{2\pi} d\phi \left[\frac{J}{2}\left(\Theta_r^2 + \frac{\sin^2\Theta}{r^2}\Phi_\phi^2\right) \right.$$
$$+ H(1 - \cos\Theta) - A\sin^2\Theta$$
$$\left. + D\left(\Theta_r \pm \frac{\sin(2\Theta)}{2r}\Phi_\phi\right)\sin\left(\alpha\frac{\pi}{2} - \phi \pm \Phi\right) \right],$$
(A2)

where $\Theta_r = \frac{d\Theta(r)}{dr}$ and $\Phi_\phi = \frac{d\Phi(\phi)}{d\phi}$ and assuming $\Theta(\mathbf{r}) = \Theta(r)$ and $\Phi(\mathbf{r}) = \Phi(\phi)$. In the last term (A2), positive sign refers to $\alpha = 1$ and 2 and negative sign refers to $\alpha = -3$. Considering $\Phi(\phi) = \zeta\phi + \eta$ with $\zeta = 1$ for $\alpha = 1, 2$ and $\zeta = -1$ for $\alpha = -3$, and $\eta = 0$ for $\alpha = 1, -3$ and $\pi/2$ for $\alpha = 2$, we find Euler equation of $\Theta(r)$ being independent of α as

$$J\left(\Theta_{rr} + \frac{\Theta_r}{r} - \frac{\sin\Theta\cos\Theta}{r^2}\right) + \frac{2D}{r}\sin^2\Theta$$
$$= H\sin\Theta - A\sin(2\Theta),$$
(A3)

where $\Theta_{rr} = \frac{d^2\Theta}{dr^2}$. The corresponding energy is given by

$$E_{sk} = 2\pi \int_0^\infty r\,dr \left[\frac{J}{2}\left(\Theta_r^2 + \frac{\sin^2\Theta}{r^2}\right) - A\sin^2\Theta \right.$$
$$\left. + H(1 - \cos\Theta) + D\left(\Theta_r + \frac{\sin(2\Theta)}{2r}\right) \right]. \quad (A4)$$

Short-distance singularity in exchange energy may be avoided with the boundary condition $\Theta(r = 0) = 0$ or π. We look for the skyrmion solution of Eq. (A3) by introducing another boundary condition $\Theta(r = \infty) = 0$ (assuming the background as a polarized ferromagnet) along with $\Theta(0) = \pi$.
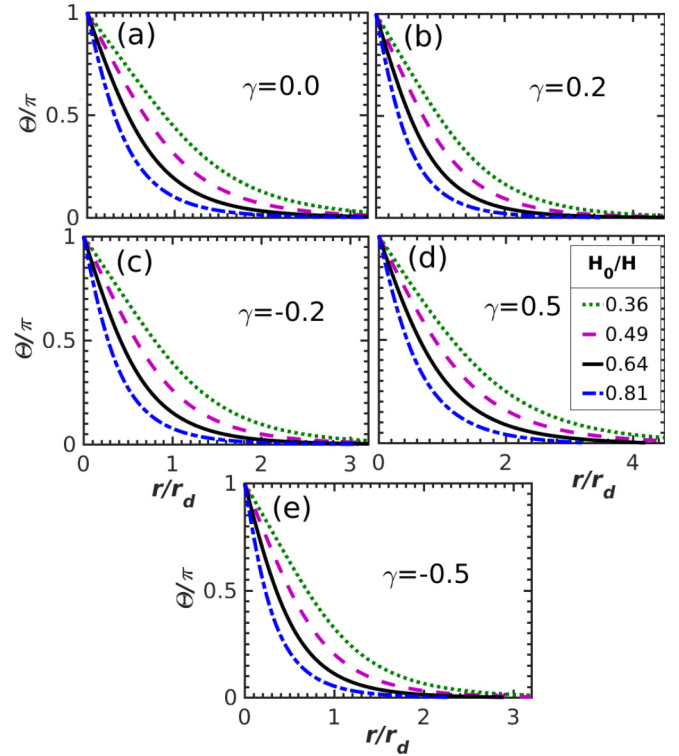

FIG. 5. Skyrmion solution: Numerical solution of the Euler equation (A8), i.e., $\Theta(r)$ vs. r/r_d for different values of γ in (a)–(e) for same set of H_0/H, viz, 0.36, 0.49, 0.64, and 0.81.

In the absence of anisotropy $(A = 0)$, an approximate and asymptotically $(r \to 0, \infty)$ exact analytical solution of Eq. (1) may be obtained as the exact solution of the simple sine-Gordon-like equation $J\frac{d^2\Theta}{dr^2} = H\sin\Theta$, i.e., $\Theta(r) = 4\arctan[\exp(-r/r_0)]$ with characteristic length scale $r_0 = \sqrt{J/H}$. Therefore, an approximate (exact for $r \to 0$ and ∞) solution for $A \neq 0$ may be obtained by considering a reduced form of Eq. (1) as $J\frac{d^2\Theta}{dr^2} = H\sin\Theta - A\sin(2\Theta)$ whose solution satisfies an integral equation

$$\int \frac{d\Theta}{\sin(\Theta/2)\sqrt{1 - \gamma\cos^2(\Theta/2)}} = -2(r/r_0) \quad (A5)$$

with $\gamma = 2A/H$ $(\gamma < 1)$, expressible into an algebraic equation

$$\sqrt{1 + \frac{2\gamma\cos(\Theta/2)}{1 - \gamma\cos(\Theta/2) + \sqrt{1-\gamma}\sqrt{1 - \gamma\cos^2(\Theta/2)}}}$$
$$\times \tan(\Theta/4) = \exp(-\sqrt{1-\gamma}\,r/r_0). \quad (A6)$$

We find the solution of Eq. (A6) as

$$\Theta(r) = 4\arctan[\exp(-g(\gamma)\,r/r_0)] \quad (A7)$$

with $g(\gamma) \simeq 1 - \frac{\gamma}{7} - \frac{\gamma^2}{30}$. However, as the smooth change in the orientation of spin depends on D, it is natural that we consider another length scale $r_d = J/D$, which is the appropriate length scale for spin spirals. By introducing r_d and transforming $r \to r_d\rho$, we find the reduced form of
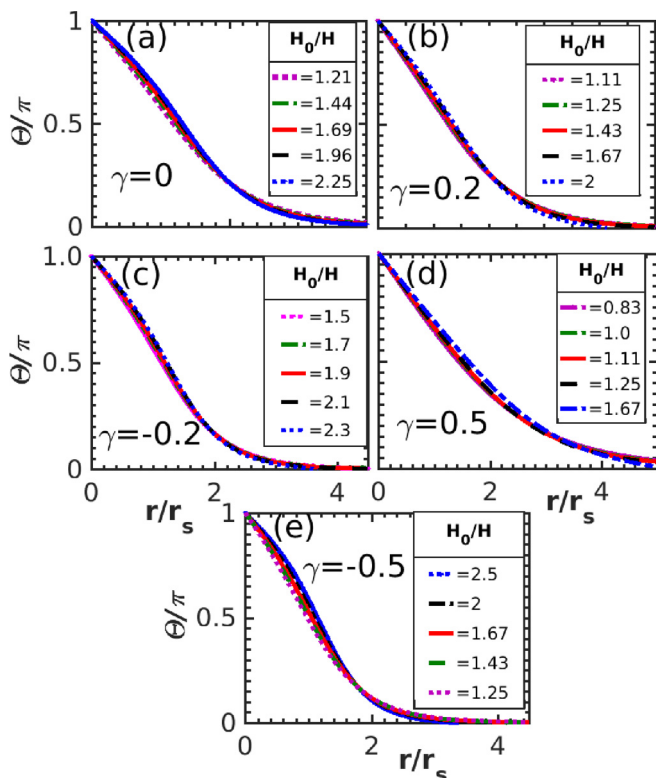
FIG. 6. Skyrmion solution: Numerical solution of the Euler equation (A9), i.e., $\Theta(r)$ vs. r/r_s for different values of γ and H_0/H in (a)–(e), covering most of the skyrmion phase shown in Fig. 3(a).

Eq. (A3) as

$$
\frac{d^2\Theta}{d\rho^2} + \frac{1}{\rho}\frac{d\Theta}{d\rho} - \frac{\sin\Theta\cos\Theta}{\rho^2} + \frac{2}{\rho}\sin^2\Theta
$$
$$
= \frac{H}{H_0}[\sin\Theta - \gamma\sin(\Theta)\cos(\Theta)], \quad (A8)
$$

where $H_0 = A_0 = D^2/J$. Numerical solution of Eq. (A8) shown in Fig. 5 for different values of the parameters H/H_0 and $\gamma = 2A/H$. We note that while the long-distance solution is independent on these parameters, the short- and intermediate-distance behavior is strongly parameter dependent, suggesting r_d is not the natural length scale of the system.

We next introduce a length scale $r_s = D/H$ and rescaling $r \to r_s\rho$, we obtain

$$
\frac{d^2\Theta}{d\rho^2} + \frac{1}{\rho}\frac{d\Theta}{d\rho} - \frac{\sin\Theta\cos\Theta}{\rho^2}
$$
$$
= \frac{H_0}{H}\left(-\frac{2}{\rho}\sin^2\Theta + \sin\Theta - \gamma\sin\Theta\cos\Theta\right) \quad (A9)
$$

whose numerical solution (Fig. 1 of the paper and Fig. 6 in this Appendix) is almost H_0/H independent for a reasonable range. We thus find natural length scale of the system as r_s. Together with the solution of $\Theta(r)$, (i) $\Phi = \phi$ for $\alpha = 1$, (ii) $\Phi = \phi + \pi/2$ for $\alpha = 2$, and (iii) $\Phi = -\phi$ for $\alpha = -3$, respectively, construct magnetic structures of Neél-type skyrmion, Bloch-type skyrmion, and Neél-type antiskyrmion.
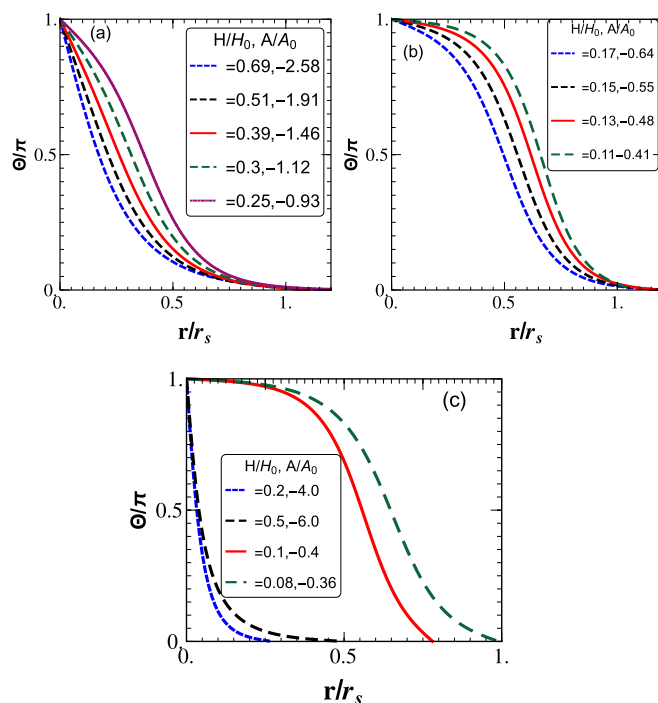

FIG. 7. Numerical solution of the Euler equation (A9), i.e., $\Theta(r)$ vs. r/r_s for different values of H/H_0 and A/A_0. The nature of the solutions changes with the parameters: These are (a) skyrmions, (b) chiral bubbles, (c) metastable skyrmions (also chiral bubbles).

However, the nature of the solution of Eq. (A9) changes with A/A_0 for low field regime. For a moderate to large H/H_0, any amount of negative (easy-axis) anisotropy provide normal skyrmion solution [Figs. 7(a)] as shown in Figs. 1 and 6. When magnetic filed is low and $|A|/A_0 \lesssim \pi/2\sqrt{2}$ (Dzyaloshinskii criterion [45] for noncollinear state at zero H), the nature of the solution is chiral-bubble-like [46], where very slow change of Θ occurs near $r = 0$, as shown in Fig. 7(b). The nature of the solution changes for $|A|/A_0 \gg \pi/2\sqrt{2}$ at low H/H_0 from chiral bubble to metastable skyrmion, as shown in Fig. 7(c), for which Θ sharply falls near $r = 0$. The behavior of metastable skyrmions are, however, fundamentally different from the normal skyrmions presented in the main text. While the normal skyrmions are appropriately scaled with r_s,
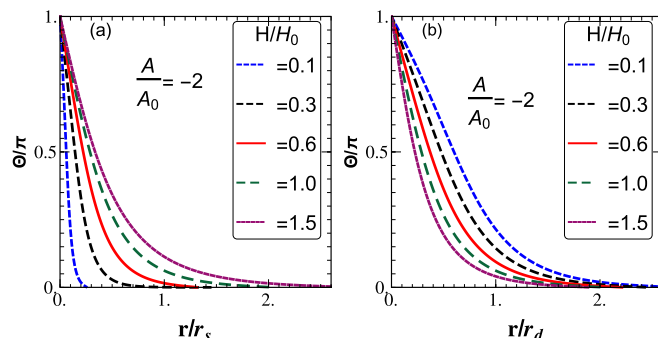

FIG. 8. Numerical solution of the Euler equations (A9) and (A8), i.e., $\Theta(r)$ vs. r/r_s and r/r_d in (a) and (b), respectively, for different values of H/H_0 and A/A_0. Clearly, these metastable skyrmion solutions are better suited with the length scale r_d.

the metastable skyrmions are better suited with the length scale r_d (see Fig. 8). Further in contrast to the metastable skyrmions, the radius of a normal skyrmion increases rapidly with the decrease of H. The metastable skyrmions are energetically unfavorable to polarized ferromagnet.

APPENDIX B: EULER EQUATION AND ITS MERON SOLUTION

The Euler equation (A3) will reduce to

$$J\left(\Theta_{rr}+\frac{\Theta_r}{r}-\frac{\sin\Theta\cos\Theta}{r^2}\right)+\frac{2D}{r}\sin^2\Theta+A\sin(2\Theta)=0 \tag{B1}$$

in the absence of magnetic field. For a sufficiently high easy-plane anisotropy ($A>0$), all the spins will align in the plane (planar ferromagnet). This indicates a boundary condition $\Theta(\infty)=\pi/2$, which together with another boundary condition $\Theta(0)=0$ or π will provide a solution for meron. By introducing a length scale $r_a=D/A$ and rescaling $r\to r_a\rho$, Eq. (B1) will reduce to

$$\frac{d^2\Theta}{d\rho^2}+\frac{1}{\rho}\frac{d\Theta}{d\rho}-\frac{\sin\Theta\cos\Theta}{\rho^2}=-\frac{A_0}{A}\left(\frac{2}{\rho}\sin^2\Theta+\sin(2\Theta)\right). \tag{B2}$$

Taking our cue from the skyrmion solution, we assume the solutions of meron is in the form

$$\Theta(r)=\pm\frac{\pi}{2}+2\arctan[\exp(-\zeta r/r_a)], \tag{B3}$$

where positive (negative) sign corresponds to spin down (up) at the center of the meron, and the parameter ζ to be determined by minimizing the corresponding energy. The energy of a meron is given by

$$E_{\text{meron}}=2\pi\int_0^\infty r\,dr\left[\frac{J}{2}\left(\Theta_r^2+\frac{\sin^2\Theta}{r^2}\right)+A\cos^2\Theta\right.$$
$$\left.+D\left(\Theta_r+\frac{\sin(2\Theta)}{2r}\right)\right], \tag{B4}$$

which may be simplified to

$$E_{\text{meron}}=\frac{J}{2}[\ln(2)+I_1]+\frac{D^2}{A}\left[\frac{\ln(2)}{\zeta^2}-\frac{I_2}{\zeta}\right], \tag{B5}$$

where $I_1=\int_0^\infty(1/r)\tanh^2(r)dr$, $I_2=\int_0^\infty(\frac{\tanh r}{\cosh r}+\frac{r}{\cosh r})dr=1+2G$, and Catalan's constant $G=\sum_{k=0}^\infty\frac{(-1)^k}{(2k+1)^2}\approx0.91$.

[1] I. E. Dzyaloshinskii, Zh. Eksp. Teor. Fiz. **32**, 1547 (1957) [Sov. Phys. JETP **5**, 1259 (1957)].

[2] T. Moriya, Phys. Rev. **120**, 91 (1960).

[3] A. N. Bogdanov and D. A. Yabionskii, Sov. Phys. JETP **68**, 101 (1989).

[4] U. K. Rößler, A. N. Bogdanov, and D. Pfleiderer, Nature (London) **442**, 797 (2006).

[5] S. Meckler, N. Mikuszeit, A. Preßler, E. Y. Vedmedenko, O. Pietzsch, and R. Wiesendanger, Phys. Rev. Lett. **103**, 157201 (2009).

[6] M. Ezawa, Phys. Rev. Lett. **105**, 197202 (2010).

[7] A. O. Leonov, T. L. Monchesky, N. Romming, A. Kubetzka, A. N. Bogdanov, and R. Wiesendanger, New J. Phys. **18**, 065003 (2016).

[8] X. Zhang, J. Xia, Y. Zhou, X. Liu, H. Zhang, and M. Ezawa, Nature Commun. **8**, 1717 (2017)

[9] T. Okubo, S. Chung, and H. Kawamura, Phys. Rev. Lett. **108**, 017206 (2012).

[10] A. Bogdanov and A. Hubert, J. Magn. Magn. Mater. **138**, 255 (1994).

[11] S. Mühlbauer, B. Binz, F. Jonietz, C. Pfleiderer, A. Rosch, A. Neubauer, R. Georgii, and P. Böni, Science **323**, 915 (2009).

[12] X. Z. Yu, N. Kanazawa, Y. Onose, K. Kimoto, W. Z. Zhang, S. Ishiwata, Y. Matsui, and Y. Tokura, Nature Mater. **10**, 106 (2011).

[13] S. Heinze, K. von Bergmann, M. Menzel, J. Brede, A. Kubetzka, R. Wiesendanger, G. Bihlmayer, and S. Blügel, Nature Phys. **7**, 713 (2011).

[14] A. Tonomura, X. Yu, K. Yanagisawa, T. Matsuda, Y. Onose, N. Kanazawa, H. S. Park, and Y. Tokura, Nano Lett. **12**, 1673 (2012).

[15] N. Romming, C. Hanneken, M. Menzel, J. E. Bickel, B. Wolter, K. von Bergmann, A. Kubetzka, and R. Weisendamger, Science **341**, 636 (2013).

[16] T. Tanigaki, K. Shibata, N. Kanazawa, X. Yu, Y. Onose, H. S. Park, D. Shindo, and Y. Tokura, Nano Lett. **15**, 5438 (2015).

[17] I. Kézsmárki, S. Bordács, P. Milde, E. Neuber, L. M. Eng, J. S. White, H. M. Ronnow, C. D. Dewhurst, M. Mochizuki, K. Yanai, H. Nakamura, D. Ehlers, V. Tsurkan, and A. Loidl, Nat. Mater. **14**, 1116 (2015).

[18] Y. Fujima, N. Abe, Y. Tokunaga, and T. Arima, Phys. Rev. B **95**, 180410(R) (2017).

[19] X. Z. Yu, Y. Onose, N. Kanazawa, J. H. Park, J. H. Han, Y. Matsui, N. Nagaosa, and Y. Tokura, Nature (London) **465**, 901 (2010).

[20] A. Chacon, L. Heinen, M. Halder, A. Bauer, W. Simeth, S. Mühlbauer, H. Berger, M. Garst, A. Rosch, and C. Pfleiderer, Nature Phys. **14**, 936 (2018).

[21] S. Das *et al.*, Nature (London) **568**, 368 (2019).

[22] A. K. Nayak, V. Kumar, T. Ma, P. Werner, E. Pippel, R. Sahoo, F. Damay, U. K. Rößler, C. Felser, and S. S. P. Parkin, Nature (London) **548**, 561 (2017).

[23] S. Jamaluddin, S. K. Manna, B. Giri, P. V. P. Madduri, S. S. P. Parkin, and A. K. Nayak, Adv. Funct. Mater. **29**, 1901776 (2019).

[24] W. Koshibae and N. Nagaosa, Nature Commun. **5**, 5148 (2014).

[25] W. Koshibae and N. Nagaosa, Nature Commun. **7**, 10542 (2016).

[26] L. Camosi, N. Rougemaille, O. Fruchart, J. Vogel, and S. Rohart, Phys. Rev. B **97**, 134404 (2018).

[27] M. Hoffmann, B. Zimmermann, G. P. Müler, D. Schürhoff, N. S. Kiselev, C. Melcher, and S. Blügel, Nature Commun. **8**, 308 (2017).

[28] S. Huang, C. Zhou, G. Chen, H. Shen, A. K. Schmid, K. Liu, and Y. Wu, Phys. Rev. B **96**, 144412 (2017).

[29] L. Camosi, S. Rohart, O. Fruchart, S. Pizzini, M. Belmeguenai, Y. Roussinné, A. Stashkevich, S. M. Cherif, L. Ranno, M. de Santis, and J. Vogel, Phys. Rev. B **95**, 214422 (2017).

[30] A. Nych, Jun-ichi Fukuda, U. Ognysta, S. Zumer, and I. Musevic, Nature Phys. **13**, 1215 (2017).

[31] X. Z. Yu, W. Koshibae, Y. Tokunaga, K. Shibata, Y. Taguchi, N. Nagaosa, and Y. Tokura, Nature (London) **564**, 95 (2018).

[32] N. Romming, A. Kubetzka, C. Hanneken, K. von Bergmann, and R. Wiesendanger, Phys. Rev. Lett. **114**, 177203 (2015).

[33] S. von Malottki, B. Dupé, P. F. Bessarab, A. Delin, and S. Heinze, Sci. Rep. **7**, 12299 (2017)

[34] S. Rohart and A. Thiaville, Phys. Rev. B **88**, 184422 (2013).

[35] X. S. Wang, H. Y. Yuan, and X. R. Wang, Comm. Phys. **1**, 31 (2018).

[36] N. Nagaosa and Y. Tokura, Nature Nanotechnol. **8**, 899 (2013).

[37] M. Vousden, M. Albert, M. Beg, Marc-Antonio Bisotti, R. Carey, D. Chernyshenko, D. Cortes-Ortuno, W. Wang, O. Hovorka, C. H. Marrows, and H. Fangohr, Appl. Phys. Lett. **108**, 132406 (2016).

[38] DMI suitable for D_n symmetric crystals, $\mathcal{E}_{DM} = -D(L_{zx}^{(y)} + L_{yz}^{(x)})$, leads to a Bloch-type skyrmionic solution with $\eta = \pi/2$.

[39] S. Banerjee, J. Rowland, O. Erten, and M. Randeria, Phys. Rev. X **4**, 031045 (2014).

[40] J. Rowland, S. Banerjee, and M. Randeria, Phys. Rev. B **93**, 020404(R) (2016).

[41] M. Hervé, B. Dupé, R. Lopes, M. Böttcher, M. D. Martins, T. Balashov, L. Gerhard, J. Sinova, and W. Wulfhekel, Nature Commun. **9**, 1015 (2018).

[42] A. O. Leonov and I. Kézsmárki, Phys. Rev. B **96**, 014423 (2017).

[43] A similar anisotropy in DMI corresponding to thin films fabricated with D_{2d} symmetric crystals given by energy density $\mathcal{E}_{DM}^- = -D(1 + \lambda \cos 2\phi)(L_{xz}^{(x)} - L_{yz}^{(y)})$ will produce similar results with reversing roles of Sks and ASks.

[44] I. S. Lobanov, H. Jónsson, and V. M. Uzdin, Phys. Rev. B **94**, 174418 (2016).

[45] I. E. Dzyaloshinskii, Sov. Phys. JETP **20**, 223 (1965).

[46] See, for example, A. Fert, N. Reyren, and V. Cros, Nature Rev. Mater. **2**, 17031 (2017).